Engineering Journal issn: 0125-8281

Article

Theoretical Study of Flexible Guided Mode Resonance Formed by Embedding Silver Nanoparticles in the Polymer Matrix for Strain Sensing Applications

Pundharika Noikorn[1,a], **Sakoolkan Boonruang**[2,b], **and Waleed S. Mohammed**[1,c,*]

1 Center of Research in Optoelectronics, Communications and Computational Systems, BU-CROCCS, School of engineering, Bangkok University, Phatumthani, 12120, Thailand
2 Opto-Electrochemical Sensing Research Team (OEC), Spectroscopic and Sensing Devices Research Group (SSDRG), National Electronics and Computer Technology Center (NECTEC), Pathum Thani 12120, Thailand
E-mail: [a]pundharika.n@gmail.com, [b]sakoolkan.boonruang@nectec.or.th, [c,*]wsoliman@gmail.com (Corresponding author)

Abstract. This paper presents a theoretical analysis of flexible guided mode resonance (GMR) structure with a configuration of an enhanced refractive index polymer nanocomposite with silver nanoparticles coated on top of a casted or imprinted grating made of the original polymer. Controlling both the volume fraction of the embedded nanoparticles (NPs) and the film thickness tunes the device sensitivity for application in mechanical lateral strain detection. The work introduces the use of the scattering matrix method (SMM) with a modification in the effective index to accurately predict the resonance wavelength peak. The results show a good agreement with rigorous coupled waves analysis (RCWA) particularly for the phase matching condition between the fundamental guided mode and diffraction. The sensitivity is calculated by perturbing the grating period due to lateral strain and correlating it to the produced wavelength shift. Using SMM for resonance wavelength calculation reduces the computational cost by a factor of 144 times while keeping a good agreement with both RCWA and the finite difference frequency domain method (FDFDM).

Keywords: Flexible guide mode resonance (GMR), embedded nanoparticles (NPs), scattering matrix method (SMM), rigorous coupled waves analysis (RCWA).

ENGINEERING JOURNAL Volume 28 Issue 8
Received 22 April 2024
Accepted 1 August 2024
Published 31 August 2024
Online at https://engj.org/
DOI:10.4186/ej.2024.28.8.33

DOI:10.4186/ej.2024.28.8.33

1. Introduction

Sensing technology has been applied over a wide range from macroscopic quantities such as temperature, strain, pressure, or flow measurement of industrial systems to smaller-scale properties of materials at a molecular level [1-3]. Among the many sensing approaches, optical sensors are commonly known for their high sensitivity [4]. The device sensitivity here indicates the response of the sensor to the amount of change in the parameter to be detected. Higher sensitivity leads to the detection of smaller changes. For several optical sensors, the working principle relies upon the presence of a grating structure, either in reflection or transmission modes [1,5]. Numerous approaches have been developed to achieve high sensitivity and better optical response. Guided mode resonance (GMR) is one of these structures [5-6]. GMR is typically formed by a grating near a higher refractive index guiding region. Sometimes the grating and the guiding region coincide [5-6]. In any GMR structure, resonance occurs when one of the film's guided modes matches one diffraction order of the grating. In that case, each complete bounce inside the film corresponds to an integer multiple of 2π phase difference. Hence, the zero order waves that leak outside constructively interfere causing a strong reflection. Changing the wavelength causes a deviation from this condition and hence the reflections drop rapidly forming a sharp peak in the spectrum. Changes in the surroundings also cause this condition to be altered and hence an obvious shift in the peak wavelength can be measured [6].

Some application examples of GMR sensors are biomedical, environmental and gas sensing [7-11]. In biomedical sensing, GMR structures are employed to detect specific biomolecules or biomarkers in biological samples. The resonance wavelength of the sensors is sensitive to changes in refractive index caused by the biomolecular binding events on the surface [7-8,11]. For environmental applications, GMR is applied to detect changes in environmental conditions such as pollution [7-8]. As for gas sensing, GMR devices can be designed for detecting specific gases through tailored resonant structures, contributing to advancements in industrial safety, environmental monitoring, and healthcare applications [9-10].

One of the main challenges of the GMR structures is to be realized on a flexible substrate to extend their applications. In optics, flexible substrates are mostly made of polymers. Polydimethylsiloxane (PDMS) is one of the most commonly used polymers due to its optical transparency as well as being non-toxic and nonflammable. Adjusting the PDMS composition and the curing agent ratio can adjust their elasticity [4]. PDMS is chemically inactive making it hard to cause any chemical reaction at the surface. It is also hydrophobic by nature making it challenging to spin coat a high refractive index film on the surface. One possible way to make the substrate temporarily hydrophilic is by breaking the chemical bonds of the polymer to reduce their contact angles [5]. Achieving a hydrophilic substrate allows the deposition of a higher index film on the flexible grating to realize the GMR device.

There is also a possibility of increasing the refractive index of the surface layer by embedding nanoparticles (NPs) into the polymer matrix. While most of the published works focus on metal oxide NPs such as tungsten oxide (WO_3) and titanium oxide (TiO_2) to increase the refractive index of the polymer, metal NPs such as silver (Ag) and gold (Au) have not been sufficiently explored for this purpose due to the presence of the plasmonic effect [12-16].

To theoretically investigate the response of the polymer-based GMR sensor with nanoparticle impurities, a model needs to be used to estimate the performance with good accuracy. Several numerical methods exist to analyze periodical structure response such as Finite Element Method (FEM), Finite Difference Time Domain (FDTD), and Finite Difference Frequency Domain (FDFD) [17-19]. The accuracy of these methods typically depends on the selection of the grid or the number of elements. Achieving higher accuracy could typically mean significant computational resources. Rigorous coupled wave analysis (RCWA) on the other hand counts on expanding the solution into a finite number of harmonics utilizing the Fourier analysis of the structure unit cell. The accuracy here depends on the selection of the number of harmonics [20]. One method that is known to break these dependencies is the scattering matrix method (SMM) [21]. SMM depends on defining the structure geometry such as the centers of scatterers or the layer's properties. The accuracy of the measurement would depend on the proper formulation of the boundary conditions rather than the number of elements or space steps. This is the reason why SMM can in general be low in computational cost and consumes fewer resources.

This paper presents a theoretical investigation of the possibility of realizing a flexible GMR structure through embedding metal NPs into a thin layer near the surface of a PDMS substrate. To avoid plasmonic absorption in the visible spectrum, the silver nanoparticles (AgNPs) will be applied in the proposed approximation model. The device sensitivity to mechanical lateral strain is studied. The effective index of the layer with embedded nanoparticles is calculated using Maxwell Garnett assuming very small particle sizes. The obtained complex refractive index is used to estimate the GMR response using the scattering matrix method and compare the results with rigorous coupled wave analysis (RCWA).

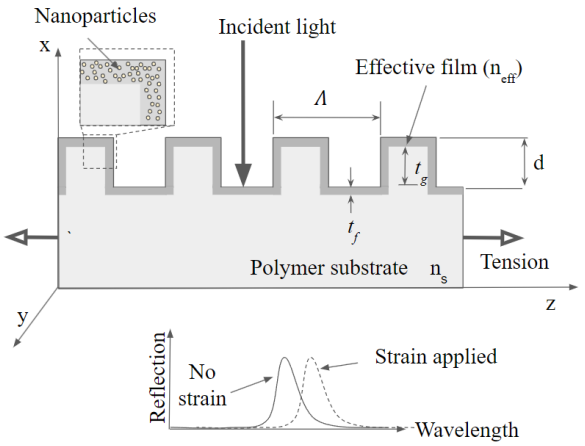

Fig. 1. The proposed configuration for flexible GMR structure with the assumption that the embedded nanoparticles are being homogeneously distributed throughout the thin film.

2. Proposed Structure Configuration and Sensing Scheme

Figure 1 shows the proposed configuration where a grating is imprinted in a flexible polymer substrate. The film is deposited by coating a higher index film formed from embedding nanoparticles in the same polymer matrix. This combination of the grating and the higher index film causes strong reflection at a specific wavelength when the diffraction order matches one of the guided modes resulting in an obvious peak in reflectance or dip in transmittance. When a lateral strain is applied to the flexible substrate, both film and grating dimensions are expected to change. This change affects the resonance condition and hence a shift in the dip wavelength is predicted as visualized in Fig. 1.

In the model approximation, if the nanoparticles' size is assumed to be small enough (<10 nm for instance) then the complex refractive index of the film (n_e) can be estimated using the effective medium theory [19].

$$n_e = n_p\sqrt{\frac{1-2V_f a}{1+2V_f a}} \tag{1}$$

where

$$a = \frac{n_m^2-n_p^2}{n_m^2+2n_p^2} \tag{2}$$

Here, n_p and n_m are the host polymer and the nanoparticle's bulk material refractive indices. The constant V_f is the nanoparticle's volume fraction. The presence of the nanoparticles increases the effective index of the film allowing the formation of a guiding region that coincides with the grating. Resonance occurs when the longitudinal propagation constant of a guided mode matches the grating vector for a specific order. This condition can be written in a simplified form as

$$\beta_q(n_e, d, \Lambda, \lambda) = m\frac{2\pi}{\Lambda} \tag{3}$$

The parameters m and q are integers and represent the diffraction order and mode index respectively. In the configuration in Fig. 1, the longitudinal constant of the q^{th} mode, β_q, depends on the effective index of the NP's film (n_{eff}), as well as the period (Λ). The thickness d is the sum of the film thickness (t_f) and the film height (t_g), $d = t_f + t_g$. This is the case as lateral strain affects both values in the same fashion. Here, the fill factor of the grating is assumed to be fixed and is not affected by the strain. When the strain is applied the grating period would increase while the film thickness and the grating height would decrease. Assuming a small stress is applied such that we can apply a perturbation theory to Eq. (3) as follows:

$$\beta_q(n_e, d+\Delta d, \Lambda+\Delta\Lambda, \lambda+\Delta\lambda) = 2\pi m\left(\frac{1}{\Lambda}-\frac{\Delta\Lambda}{\Lambda^2}\right) \tag{4}$$

Assuming small changes in the parameters, we can expand the left side of Eq. (4) as

$$\begin{aligned}&\beta_q(n_e, d+\Delta d, \Lambda+\Delta\Lambda, \lambda+\Delta\lambda)\\ &\quad\approx \beta_q(n_e, d, \Lambda, \lambda) + \Delta d\frac{\partial\beta_q}{\partial d} + \Delta\Lambda\frac{\partial\beta_q}{\partial\Lambda} + \Delta\lambda\frac{\partial\beta_q}{\partial\lambda}\end{aligned} \tag{5}$$

Using this expansion in Eq. (4),

$$\begin{aligned}&\beta_q(n_e, d, \Lambda, \lambda) + \Delta d\frac{\partial\beta_q}{\partial d} + \Delta\Lambda\frac{\partial\beta_q}{\partial\Lambda} + \Delta\lambda\frac{\partial\beta_q}{\partial\lambda}\\ &\quad= \frac{2\pi m}{\Lambda} - 2\pi m\frac{\Delta\Lambda}{\Lambda^2}\end{aligned} \tag{6}$$

If the wavelength is in the vicinity of the resonance condition, $\lambda \approx \lambda_p$ where λ_p is the resonance wavelength, then the first term on the left side cancels the first term on the right side and we can re arrange Eq. (6) as

$$\Delta\lambda_p = -\frac{1}{\partial\beta_q/\partial\lambda}\left[\Delta d\frac{\partial\beta_q}{\partial d} + \Delta\Lambda\left(\frac{\partial\beta_q}{\partial\Lambda}+\frac{2\pi m}{\Lambda^2}\right)\right] \tag{7}$$

The expression in Eq. (7) shows the change of the resonance wavelength due to the changes in both film depth and grating period. The first term, $\partial\beta_q/\partial\lambda$, is the modal dispersion around the resonance condition. Increasing the excitation wavelength pushes the waveguide towards single mode condition and hence β_q is expected to decrease. The derivative is then negative. Increasing the thickness of the film on the other hand pushes the waveguide towards multimode condition and hence β_q is expected to increase. The term $\partial\beta_q/\partial d$ is then expected to be positive. The change of β_q with the period can be neglected as the fill factor remains constant, then the effective index of the grating region can be to the first order approximation remain constant. Equation (7) can then be simplified as

$$\Delta\lambda \approx \frac{1}{|\partial\beta_q/\partial\lambda|}\left[\Delta d\left|\frac{\partial\beta_q}{\partial d}\right| + \Delta\Lambda\left(\frac{2\pi m}{\Lambda^2}\right)\right] \tag{8}$$

Applying lateral strain, the thickness is expected to decrease, $\Delta d = -|\Delta d|$, while the period is expected to increase, $\Delta\Lambda = |\Delta\Lambda|$.

$$\Delta\lambda \approx \frac{1}{|\partial\beta_q/\partial\lambda|}\left[-|\Delta d|\left|\frac{\partial\beta_q}{\partial d}\right| + |\Delta\Lambda|\left(\frac{2\pi m}{\Lambda^2}\right)\right] \quad (9)$$

Inspecting, Eq. (9), one can indicate that two opposite effects are caused by lateral strain. The reduction of the thickness causes a blue shift while the increase in the period causes a red shift. The total shift in the resonance wavelength then depends on the dominant effect. If we assume that the tension applied causes small deformation [23], then

$$v\frac{\Delta\Lambda}{\Lambda} \approx -\frac{\Delta d}{d} \quad (10)$$

where v is the Poison's ratio for the polymer ($v \approx 0.4$ for PDMS) [24]. Using this approximation in Eq. (9)

$$\Delta\lambda \approx \frac{\Delta\varepsilon}{|\partial\beta_q/\partial\lambda|}\left(\frac{2\pi m}{\Lambda} - vd\left|\frac{\partial\beta_q}{\partial d}\right|\right) \quad (11)$$

where $\Delta\varepsilon = \frac{|\Delta\Lambda|}{\Lambda}$ is the longitudinal strain and d is the grating waveguide film's thickness at zero strain. The sensitivity in terms of strain can be written as

$$S_\varepsilon = \frac{\Delta\lambda}{\Delta\varepsilon} \approx \frac{1}{|\partial\beta_q/\partial\lambda|}\left(\frac{2\pi m}{\Lambda} - vd\left|\frac{\partial\beta_q}{\partial d}\right|\right) \quad (12a)$$

The sensitivity can also be written in terms of the stress in the polymer as a result of the applied tension as $\Delta\varepsilon = \Delta\sigma E$, where σ is the stress and E is the Young's modulus constant for the polymer (typical values range from 1.6 to 2.0 MPa depending on the curing process) [25]. According to Eq. (11), the applied tension on the polymer substrate can result in a resonance red-shift when $\left|\frac{\partial\beta_q}{\partial d}\right| < \frac{2\pi m}{v\Lambda d}$. The resonance wavelength at weak tension force is expected to act in an almost linear way assuming the derivatives $\partial\beta_q/\partial\lambda$ and $\partial\beta_q/\partial d$ are almost constant around that condition. The device's sensitivity in terms of nm per MPa is

$$S_\sigma = \frac{\Delta\lambda}{\Delta\sigma} \approx \frac{\mathrm{E}}{\left|\frac{\partial\beta_q}{\partial\lambda}\right|}\left(\frac{2\pi m}{\Lambda} - vd\left|\frac{\partial\beta_q}{\partial d}\right|\right) = \mathrm{E}\, S_\varepsilon \quad (12b)$$

To test this approximate model for flexible GMR structure, one needs to use a reliable reference method for sensitivity calculations. Rigorous coupled wave analysis (RCWA) is known for its high accuracy when used for GMR structures [20]. Hence, RCWA is used as a main checkpoint to calculate the resonance wavelength at different structure dimensions due to strain and compare it to the result from Eq. (12b). However, using RCWA for sensitivity calculation typically requires a long computational time especially when scanning over multiple parameters such as wavelength, thickness, and nanoparticle volume fraction. As the target of this proposed approximate model is to provide a fast design tool, we propose the use of a faster model for both structure modal analysis and resonance wavelength calculation utilizing the scattering matrix method (SMM).

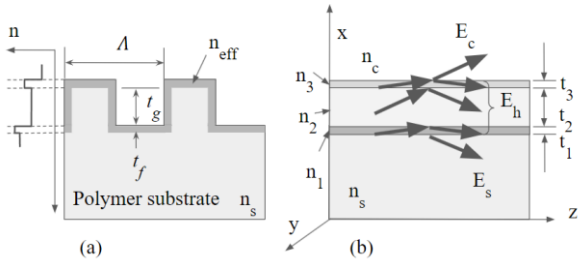

Fig. 2. (a) Representation of GMR in the form of homogeneous layers each with an effective index. (b) Plane wave representation of the field inside the layers.

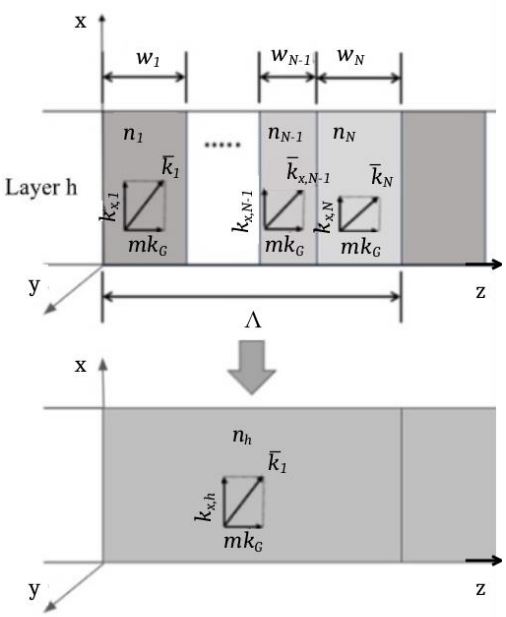

Fig. 3. Effective medium representation of a periodical layer where each unit cell is represented as a collection of homogeneous segments.

It is worth noting that in the model presented in Eq. (12b), the strain effect is assumed to only change the dimension of the structure while neglecting the effect in the refractive index. The assumption is made based on the intended strain limits targeted here (within 10%).

3. Model Analysis Using Scattering Matrix Approach

3.1. Effective Medium Calculation

To solve for the guided modes inside the GMR structure, the structure is presented here as a multiple uniform layer as in Fig. 2. Finding the effective index of each layer can be properly done using RCWA. However, one of the main goals of this work is to provide a faster calculation tool that can provide results as close as possible to RCWA with a fraction of the computation time. One common approximation is the use of effective medium theory (EMT) [22] where the index can be approximated by

$$n_h = \sum_{j=1}^{N_h} \frac{n_{j,h} w_{j,h}}{\Lambda} \quad (13)$$

Here each layer, h, is assumed to be formed by several homogeneous segments, N_h, as demonstrated in Fig. 3. The constants $n_{j,h}$ and $w_{j,h}$ are the index and width of the j^{th} homogeneous segment in the h^{th} layer. The constant Λ is the period

The main issue with Eq. (13) is that it is driven based on the assumption of a plane wave propagation along the z axis inside the layer. The accumulated phase in this case is $\phi_h = \frac{2\pi}{\lambda}\sum_{j=1}^{N_h} n_{j,h}w_{j,h} = \frac{2\pi}{\lambda}n_h\Lambda$ However, diffracted light inside each region propagates with a wavenumber $\bar{k}_j = mk_G\hat{z} + k_{x,j}\hat{x}$, where j is the homogenous region index inside the unit cell and m is the diffraction order. That corresponds to the following dispersion equation.

$$k_j^2 = \left(\frac{2\pi n_j}{\lambda}\right)^2 = m^2k_G^2 + k_{x,j}^2 \tag{14}$$

Here, k_G is the grating wavenumber and it equals $\frac{2\pi}{\Lambda}$. Similarly, inside the effective region, the dispersion equation is $k_h^2 = \left(\frac{2\pi n_h}{\lambda}\right)^2 = m^2k_G^2 + k_{x,h}^2$. When the grating period is small enough (k_G is large), then we could assume that light covers a displacement of $\bar{r}_j = x_j\hat{x} + t_j\hat{z}$ when propagating inside the j^{th} segment. Here t_j is the segment thickness and x_j is the distance along x axis. The direction of the plane wave propagation can be estimated as

$$\tan\theta = \frac{x_j}{t_j} = \frac{k_{x,j}}{mk_G} \rightarrow x_j = t_j\frac{k_{x,j}}{mk_G} \tag{15}$$

Similarly, we could write $x_h = \Lambda\frac{k_{x,h}}{mk_G}$ for the effective unit cell. The total phase due to light propagation along the diffraction order inside the regions can be approximated as

$$\phi_h = \sum_{j=1}^{N_h}\bar{k}_j\cdot\bar{r}_j = \sum_{j=1}^{N_h}\left(mk_Gt_j + k_{x,j}x_j\right) \tag{16}$$

Using the relation in Eq. (15), we can write the accumulated phase as

$$\phi_h = \sum_{j=1}^{N_h}\frac{t_j}{mk_G}\left(m^2k_G^2 + k_{x,j}^2\right)\sum_{j=1}^{N_h}\frac{d_j}{mk_G}\left(\frac{2\pi n_j}{\lambda}\right)^2 \tag{17}$$

The simplification in Eq. (17) is achieved using the dispersion relation in Eq. (13). This phase should be equivalent to the one generated by light propagation through the full unit cell of the effective medium. In other words, $\phi_h = \sum_{j=1}^{N_h}\frac{t_j}{mk_G}\left(\frac{2\pi n_j}{\lambda}\right)^2 = \frac{\Lambda}{mk_G}\left(\frac{2\pi n_h}{\lambda}\right)^2$. Hence, the effective index of the h^{th} layer can be approximated, when considering propagation along the diffraction order, as

$$n_h = \sqrt{\sum_{j=1}^{N_h}\frac{t_j}{\Lambda}n_j^2} \tag{18}$$

In contrast to Eq. (13), the effective index in Eq. (18) is calculated from averaging the permittivity ($\varepsilon_j = n_j^2$) of the media forming the unit cell instead of the index. One remaining issue here is that the derivation used to obtain Eq. (18) does not include the multiple coupling effect between the different diffraction orders. To partially compensate for such an effect, we can state a hypothesis that the effective index in Eq. (18) should be in a more generic form as

$$n_h = \left(\sum_{j=1}^{N_h}\frac{t_j}{\Lambda}n_j^b\right)^{1/b} \tag{19}$$

Constant b is a power factor that needs to be optimized to minimize the deviation of the SMM from the RCWA calculations. This representation in Eq. (19) seems to fit the TE polarization. Setting b to -2 gives the known effective index representation for the TM case. However, in this paper, the constant b is varied to match the first order resonance to that of the RCWA.

3.2. Scattering Matrix Formation

Using the effective medium approximation in the previous section, we can now construct a multilayer structure as in Fig. (2b). To solve for the guided modes inside the GMR layers, the electrical/magnetic field inside each layer is assumed to be a summation of two plane waves as in Fig. (2b). To ensure guidance, the field at the substrate and the cladding layers are assumed to have one plane wave component each as depicted in Fig. (2b). For the case of TE polarization, the y component of the electric field can be expressed as follows:

$$E_y(x,z) = \begin{cases} A_ce^{ik_{x,c}(x-t_N)-i\beta z}, & x > x_N \\ A_he^{ik_{x,h}(x-t_{h-1})-i\beta z} + B_he^{-ik_{x,h}(x-t_{h-1})-i\beta z}, & x_h \le x \le x_{h+1} \\ B_se^{-ik_{x,s}x-i\beta z}, & x < 0 \end{cases} \tag{20}$$

Here, A's and B's are constant coefficients. The suffices s and c indicate substrate and cladding respectively. The index h varies from 1 to N-1 where N is the total number of layers. The x component of the wave vector inside each layer is $k_{x,l} = \sqrt{k_o^2n_l^2 - \beta^2}$, where β is the longitudinal component of the wave vector. The index l can be s, c, or h where h varies from 1 to N-1. The z component of the magnetic field can be extracted as $H_z = -\frac{1}{i\omega\mu_o}\frac{\partial E_y}{\partial x}$. For the case of the TM polarization, the y component of the magnetic field will be represented by Eq. (20) instead. The relationship between E_z and H_y is however $E_z = \frac{1}{i\omega\varepsilon}\frac{\partial H_y}{\partial x}$. Applying the boundary conditions between each layer we can derive the following relation between the field coefficients in the superstrate and substrate.

$$\begin{bmatrix} m_{11} & m_{12} \\ m_{21} & m_{22} \end{bmatrix}\begin{bmatrix} 1 \\ \eta_sk_{x,s} \end{bmatrix}B_s = e^{ik_{x,c}x_N}\begin{bmatrix} 1 \\ -\eta_ck_{x,c} \end{bmatrix}A_c \tag{21}$$

where

$$\begin{bmatrix} m_{11} & m_{12} \\ m_{21} & m_{22} \end{bmatrix} M_N M_{N-1} \cdots M_2 M_1 \begin{bmatrix} 1 & 1 \\ \eta_1 k_{x,1} & -\eta_1 k_{x,1} \end{bmatrix}^{-1} \quad (22)$$

And

$$M_h = \begin{cases} \begin{bmatrix} 1 & 1 \\ \eta_{h+1} k_{x,h+1} & -\eta_{h+1} k_{x,h+1} \end{bmatrix}^{-1} \\ \begin{bmatrix} e^{ik_{x,h}d_h} & e^{-ik_{x,h}d_h} \\ \eta_h k_{x,h} e^{ik_{x,h}d_h} & -\eta_h k_{x,h} e^{ik_{x,h}d_h} \end{bmatrix}, \quad h < N \\ \begin{bmatrix} e^{ik_{x,N}d_N} & e^{-ik_{x,N}d_N} \\ -\eta_N k_{x,N} e^{ik_{x,N}d_N} & \eta_N k_{x,N} e^{-ik_{x,N}d_N} \end{bmatrix}, h = N \end{cases} \quad (23)$$

The constant $\eta_j = 1$ for TE polarization and $\eta_j = n_j^2$ for TM polarization. Equation (21) represents two linear equations, the solution of which produces the following characteristic equation.

$$(m_{21} + \eta_s k_{x,s} m_{22}) + \eta_c k_{x,c} (m_{11} + \eta_s k_{x,s} m_{12}) = 0 \quad (24)$$

The left side of Eq. (24) is a function of β as well as the structure parameters and wavelength. For specific structure parameters and launching wavelength, any guided mode should have a value of β that makes the right side of Eq. (24) equal zero. Notice that using embedded metal nanoparticles yield a complex effective index. Hence, the left side of Eq. (24) is generally complex. To simplify the analysis, instead of finding the zeros, the guided modes could be found by searching for β values that minimize the absolute of the left side,

$$Sm(\beta_q) = \left| \begin{matrix} (m_{21} + \eta_s k_{x,s} m_{22}) + \\ \eta_c k_{x,c} (m_{11} + \eta_s k_{x,s} m_{12}) \end{matrix} \right| \to 0 \quad (25)$$

The function *Sm* is referred to as the scattering function and β_q is the propagation constant of the q^{th} guided mode.

3.3. Scattering Matrix Method for GMR Analysis

When modelling GMR structures and their application in sensing, we are mainly interested in finding the resonance wavelengths and their change with the surroundings. The model in Eq. (25) returns the guided modes in a multilayer structure. This can be modified using the relation for resonance wavelength in Eq. (3) to directly solve for the resonance wavelengths. Noted here that the following analysis focuses on light excitation at normal incidents. At resonance, the longitudinal component of the wave vector is $\beta_q = mk_G$, where $k_G = \frac{2\pi}{\Lambda}$. Here, the q^{th} guided mode is assumed to match the m^{th} diffraction order. This condition is satisfied only at the resonance wavelength, λ_p. Hence, the dispersion relation inside each layer becomes $k_{x,l} = \sqrt{(2\pi n_l/\lambda_p)^2 - (mk_G)^2}$. Using this relation in Eq. (24) results in a scattering matrix that is a function of the peak wavelength. The peak wavelength of the GMR structure can then be approximated as a solution to the following minimization.

$$Sm(\lambda_p) = \left| \begin{matrix} [m_{21}(\lambda_p) + \eta_s k_{x,s}(\lambda_p) m_{22}(\lambda_p)] \\ +\eta_c k_{x,c}(\lambda_p) \dots \\ [m_{11}(\lambda_p) + \eta_s k_{x,s}(\lambda_p) m_{12}(\lambda_p)] \end{matrix} \right| \to 0 \quad (26)$$

The approximate sensitivity in Eq. (12b) is defined around the resonance condition. Hence, for a peak wavelength obtained from Eq. (26) at a specific structure parameter, the derivatives $\partial\beta_q/\partial\lambda$ and $\partial\beta_q/\partial d$ can be estimated by solving Eq. (25) at wavelength values around λ_p and thicknesses around the zero-strain film thickness, d_o, as

$$\frac{\partial \beta_q}{\partial \lambda} \approx \frac{\beta_q(\lambda_p + \delta\lambda, d) - \beta_q(\lambda_p - \delta\lambda, d)}{2\delta\lambda} \quad (27a)$$

$$\frac{\partial \beta_q}{\partial d} \approx \frac{\beta_q(\lambda_p, d + \delta d) - \beta_q(\lambda_p, d - \delta d)}{2\delta d} \quad (27b)$$

Here, $\delta\lambda$ and δd are small wavelength and grating-waveguide film's thickness deviations. These values can be set as $0.1\lambda_p$ and $0.1d$ respectively. Using the values obtained in Eq. (27a) and (27b), one can estimate the device sensitivity proposed in Eq. (12b). Another way to obtain the perturbation is through applying small lateral strains, $\delta\varepsilon$ and $-\delta\varepsilon$ that cause resonance wavelengths of $\lambda_p(\varepsilon + \delta\varepsilon)$ and $\lambda_p(\varepsilon - \delta\varepsilon)$ respectively. The sensitivity in Eq. (12a) can be calculated as

$$S_\varepsilon = \frac{\Delta\lambda}{\Delta\varepsilon} \approx \frac{\lambda_p(\varepsilon + \delta\varepsilon) - \lambda_p(\varepsilon - \delta\varepsilon)}{2\delta\varepsilon} \quad (28)$$

Maximum sensitivity is expected to be at cut-off condition when $\beta \to 2\pi n_s/\lambda$ [26]. In this case the propagation constant is independent of the film thickness variation, $\frac{\partial\beta}{\partial d} = 0$ and $\frac{\partial\beta}{\partial\lambda} = -\frac{2\pi n_s}{\lambda^2}$. The resonance wavelength from Eq. (3) becomes.

$$\beta = \frac{2\pi m}{\Lambda} \to \lambda_{p,c} = n_s \Lambda \quad (29)$$

Here, $\lambda_{p,c}$ is the resonance wavelength at the cut off condition. In this case, the derivative $\frac{\partial\beta}{\partial\lambda}\Big|_{\lambda_P}$ becomes $-\frac{2\pi}{n_s \Lambda^2}$. The maximum value of the sensitivity in Eq. (12a) is

$$S_{\varepsilon,max} \approx \mathrm{m} n_s \Lambda \quad (30)$$

In terms of strain in %, the maximum sensitivity becomes $mn_s\Lambda/100$.

3.4. Structure Representation

For the structure of interest in Fig. 2, we can write the effective indices of each region as

$$n_h = \begin{cases} \left(n_e^b \cdot ff + (1 - ff)\right)^{1/b} & h = 3 \\ \left(n_s^b \cdot ff + (1 - ff)\right)^{1/b} & h = 2 \\ \left(n_s^b \cdot ff + n_e^b \cdot (1 - ff)\right)^{1/b} & h = 1 \end{cases} \quad (31)$$

The constant *ff* is the fill factor of the grating. The difference $\Delta ff = 1 - 2ff$. Recall that n_e is the effective index of the polymer with AgNPs embedded in it. This value changes for different values of the particles' volume fractions. The surrounding index is assumed to be air, n = 1. The substrate index is assumed to be the same polymer as the host region. In our analysis, we assume the host polymer to be PDMS with a fixed refractive index of n_s = 1.43. The resonance wavelengths in the following sections are calculated for the TM polarization.

As mentioned earlier the expression in Eq. (31) seems to fit for TE polarization for positive values of b while negative values seem to fit the TM polarization. In the following sections, the work aims to test the efficiency of using SMM to calculate the GMR response in terms of accuracy and computational cost reduction. It also examines the suitability of applying the perturbation model to estimate the device sensitivity to strain and optimize the design parameters.

It is worth mentioning SMM is a well-known method and has been presented in many literatures. The paper utilizes the efficiency of this method by enforcing the resonance condition into the matrix and modifying the effective index to match the more accurate RCWA analysis. That minimizes the computational time required for sensitivity analysis and device design optimization.

4. Model Verification

In this section, RCWA is used as a reference to test the accuracy of the scattering matrix approximation when solving for the resonance wavelength of the GMR structure. The model high index film is assumed to be prepared by embedding AgNPs in PDMS. The complex effective index of the high index film is calculated using effective medium theory (in Eq. (1)-(2)) and used in both RCWA and the proposed scattering matrix models. The RCWA model calculates the reflection spectrum of the structure. The presence of resonance is indicated by a Lorentzian shape peak. Here, the complex values of the refractive index of Ag were obtained from Jonson and Christy 1972 [27].

The resonance properties of the structure can then be defined by the wavelength of the peak, λ_p. The resonance condition, however, for the scattering matrix should minimize the left side of Eq. (26). When plotting *Sm* versus wavelength, resonance wavelengths are those that correspond to the minimum in the graph. Hence, when comparing RCWA calculations to the scattering matrix, we will be comparing the presence of peaks in the reflection spectrum from the RCWA to the corresponding minima in the scattering matrix. Finally, for easier signal processing and visualization, it is more practical to plot the log of *Sm*. This comparison is depicted in Fig. 4 for a GMR structure comprised of PDMS substrate (n = 1.43), period of 450 nm, grating depth of 500 nm, and high index film thickness of 400 nm. The fill factor of the grating is 0.5 and the volume fraction of AgNPs in the high index film varies from 0.1 to 0.2. In calculating the effective index of the layers as in Eq. (28), the power factor (b) is set to 2. That follows the assumption in Eq. (19). When comparing to FDFD calculation, the fundamental mode shows the spectrum that has a resonance that agrees with both RCWA and SMM under the same condition however for higher modes, more accuracy is required for FDFD hence more calculation time would be needed to show a smoother graph.

It is worth mentioning that for the presented GMR structure, there is a minimum limit of the volume fraction on the nanoparticles that is needed to support a guided mode. That is when the propagation constant becomes at the cut off condition, $\beta_{c.o.} = \frac{2\pi}{\lambda} n_s$. The characteristic equation for TM at cut off condition can be approximated as $tan(\kappa_{c.o.} d) = \frac{n_e^2 \gamma_{2,c.o.}}{n_c^2 \cdot \kappa_{c.o.}}$, where, $\gamma_{2,c.o.} = \frac{2\pi}{\lambda}\sqrt{n_s^2 - n_2^2}$ and $\kappa_{c.o.} = \frac{2\pi}{\lambda}\sqrt{n_1^2 - n_s^2}$; where n_1 and n_2 are the refractive indices of layers 1 and 2 respectively. As an example, for a polymer structure with a period of 450 nm and film thickness of 400 nm, the minimum volume fraction obtained is 0.04.

Figure 4 shows a good correspondence between the RCWA reflection peaks and the dips in the absolute of the scattering matrix. There is however a noticeable deviation especially for larger volume fractions of AgNPs and for resonances due to higher order modes. This discrepancy is expected as the model, unlike RCWA, does not take into consideration the multiple coupling between the diffraction orders within the grating.

This comparison is visualized in Fig. 5 where three different cases are considered: b=1, b=2, and b=2.4. The case when b=1 corresponds to the effective index method in Eq. (13) and it experiences the largest deviation from the RCWA in both orders. In comparison, when b=2, as in Eq. (18), the error in both orders is dramatically reduced. The slopes of both orders still show obvious differences. To correct the error in the scattering matrix calculation, we plotted the average mean square error for both orders as a function of the power factor varying from b=1 to b=3 as depicted in the inset.

The plots show that the minimum error for the fundamental mode is at b=2.4 while that of the first higher order mode is at b=1.9. For the case of b=2.4, the calculated resonance due to the fundamental mode using SMM is almost identical to RCWA. However, the deviation in the first higher order mode increases compared to b=2. For higher value of b the error increases as shown in the inset in Fig. 5. In both cases, however, the error of the slope between RCWA and SMM is high for the higher order mode. This could be mainly because of deriving the relation in Eq. (18) and (19), k_G was assumed to be much larger than k_x inside the layer. This is not necessarily the case for the higher order modes. Notice that the optimum value of b is positive while it was expected to be closer to -2.

DOI:10.4186/ej.2024.28.8.33

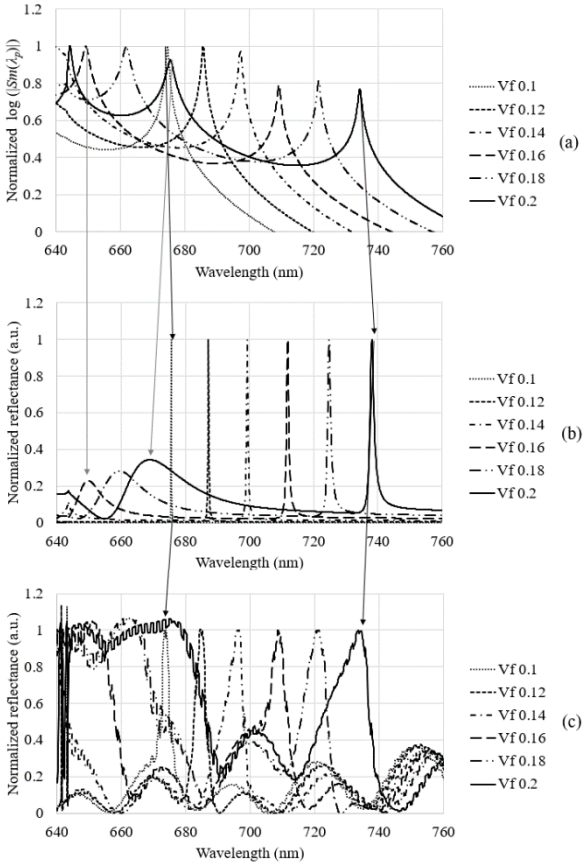

Fig. 4. (a) Change of $1 - log\left(Sm(\lambda_p)\right)$ with the volume fraction of the AgNPs in the PDMS matrix the form the high index film from 0.1 to 0.2. The film thickness (t_f) is set to 400 nm, and the grating height (t_g) is 500 nm. The period is 450 nm and the fill factor is 0.5. (b) Calculated RCWA normalized reflectance for the same structures. (c) Calculated FDFD normalized reflectance for the same structures.

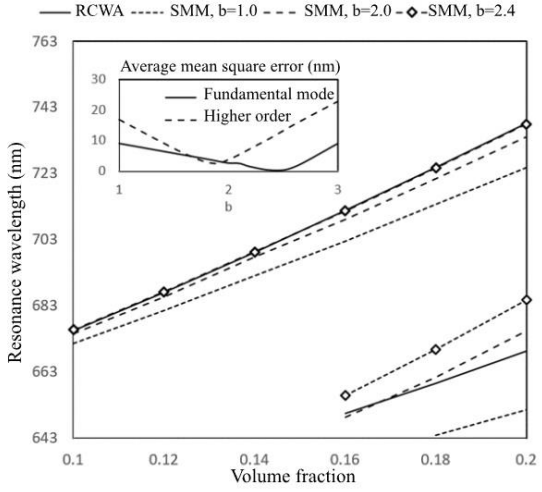

Fig. 5. The resonance wavelength for the coupling between fundamental mode (upper set) as well as the first higher (lower set) with the first grating diffraction order. Their power indices are shown when calculating the effective index of each layer: b=1, b=2 and b=2.4.

Table 1. Comparison of the computational cost between RCWA, FDFD and SMM for the same structure parameters and scanning range.

	RCWA	**FDFD**	**SMM**
Number of wavelength points	1601	1601	1601
Wavelength range (nm)	640-800	640-800	640-800
Number of harmonics	61	61	61
Time per strain point (s)	168	459	-
Total calculation time for six points (s)	1008	13,958	7
Ratio/SMM	144	1994	1

Notice that in order to compare peak to peak in Fig. 4, the graph for scattering method was plotted as $1 - log(Sm)$ versus the wavelength. Hence the peaks are compared to GMR and FDFD.

It is worth mentioning that the computational time for generating the plots using SMM was 144 times faster than RCWA using AMD Ryzen 5 3550H with Radeon Vega Mobile Gfx 2.10 GHz processor and 24 GB RAM computer. While for FDFD, SMM was 1994 times faster. The calculation cost is shown in Table 1 when comparing both models for the same structure and parameters.

From the results in Fig. 5, one could safely focus only on utilizing the fundamental mode of the proposed GMR structure for the desired strain sensing and set the power factor b to 2.4. The effect of stress can be studied by varying the grating period and using Eq. (10) to calculate the changes in the thickness of all the layers. In this case, the SMM method can be efficiently used to produce faster results and with acceptable accuracy.

5. Results

5.1. GMR Response under Strain

The effect of strain is applied by increasing the lateral dimension of the unit cell while decreasing the thickness of the layers using the ratio in Eq. (10) when v is set to 0.4. The plots in Fig. 6 show a strong correlation between the SMM calculations and RCWA for the fundamental mode when increasing the strain from 0% to 6.7%. In this case, the period of the grating increases from 450 to 480 nm with 10 nm steps. The plots in the figure show a clear agreement between SMM and RCWA in different GMR configurations by varying the volume fraction of AgNPs from 0.1 to 0.2. The plots in the figure are calculated for a

film thickness of 400 nm. Note that the slope of each plot represents the sensitivity of the device to strain at the given NPs' volume fraction.

In Fig. 6, the effect of lateral strain on the resonance peak for different AgNPs concentrations in the polymer film when comparing RCWA to SMM with *b*=2.4 for the first order diffraction. At film thicknesses of 400 nm, grating height of 500 nm, fill factor of 0.5, and varied volume fraction of the AgNPs from 0.1 to 0.2. The grating period is 450-490 nm.

The device sensitivity to strain is calculated at different film thicknesses (*tf*) using SMM and RCWA as depicted in Fig. 7. Here, the amount of strain was varied from 0 to 11% and the slope of the obtained peak wavelength shift was calculated for each volume fraction of AgNPs inside the polymer which forms the high index film. The film thicknesses (*tf*) of 400 nm and 600 nm were compared to RCWA calculations. The results show good agreement between both methods in terms of sensitivity values as well as the trend of the change in the device sensitivity with the volume fraction. It is worth noting that the device sensitivity over the given volume fraction range experiences a deviation of 3.4% from RCWA, which is for the case of 300 nm film thickness. The film thickness of 400 nm shows minimal sensitivity change versus the volume fraction in both SMM (0.9%) and RCWA (1.7%). At film thickness of 500 nm, both RCWA and SMM show a change of 1.7% but with the opposite sign compared to 400 nm.

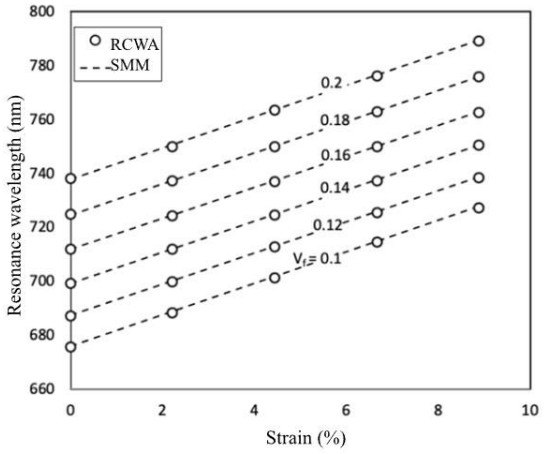

Fig. 6. The effect of lateral strain on the resonance peak for different AgNPs concentration in the polymer film when comparing RCWA to SMM with *b*=2.4 for the first order diffraction. At film thicknesses 400 nm, grating height of 500 nm, fill factor of 0.5 and varied volume fraction of the AgNPs from 0.1 to 0.2. The grating period is 450-490 nm.

5.2. Approximate Model Calculations

In the plots in Fig. 7, the sensitivity was calculated by estimating the slope of the wavelength peak versus strain curve when calculated using SMM in comparison to RCWA. This section compares the results when using the approximations in Eq. (12a) and 28 and examines if the results follow the maximum sensitivity limit defined by Eq. (30). Figure 8(a) shows the comparison between RCWA, SMM, and the approximations for 400 nm thick polymer film with AgNPs impurities. In all the calculations, the grating depth is set to be $t_g = t_f + 100\ nm$. In this case, for 400 nm film, the grating depth is 500 nm. The volume fraction of the particles varies from 0.01 to 0.2. The substrate is made of the same polymer material of index 1.43 and the grating has a 450 nm period. The plots show a good match between the SMM and the RCWA. The approximations in Eq. (28) and (12a) show a good match, especially at smaller values of the volume fraction. Deviations up to 3% are observed at larger volume fraction values. This error is mainly due to ignoring higher order effect as well as multiple coupling effect. It is worth mentioning that for the model in Eq. (12), however, a correction factor was multiplied by the right side in order to sustain the sensitivity limit in Eq. (30).

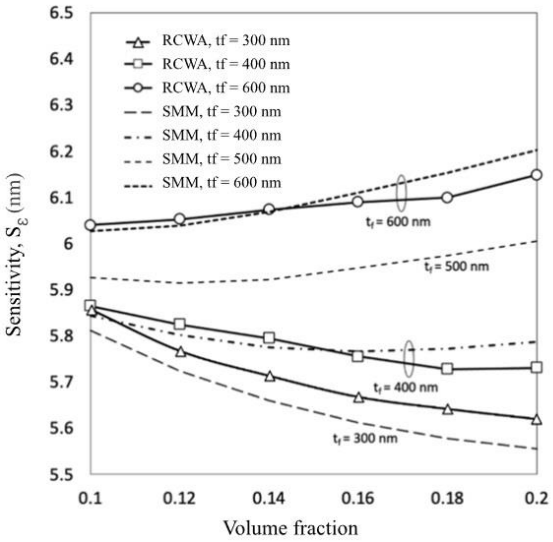

Fig. 7. Calculated sensitivity, *Sε*, for different high refractive index polymer film thicknesses when varying the volume fraction of the AgNPs from 0.1 to 0.2 using the SMM method. The curves for film thicknesses of 400 nm and 600 nm are compared to RCWA. The lateral strain being applied here is from 0 to 11%, the grating height is 500 nm, the fill factor is 0.5, and the grating period is 450-500 nm.

$$S_\varepsilon \approx \eta \frac{1}{|\partial\beta_q/\partial\lambda|}\left(\frac{2\pi m}{\Lambda} - vd\left|\frac{\partial\beta_q}{\partial d}\right|\right) \tag{32}$$

The correction constant is obtained when setting the sensitivity to the maximum limit at the modal cut off condition in the high index region. At cut off, the propagation constant is $\beta_{q,c.o.} = 2\pi n_s/\lambda$ and it does not change with thickness. Hence, $\frac{\partial\beta_q}{\partial d}\Big|_{c.o.} = 0$ an $\frac{\partial\beta_q}{\partial\lambda}\Big|_{c.o.} = \frac{2\pi}{\lambda}\left(\frac{\partial n_s}{\partial\lambda} - \frac{n_s}{\lambda}\right)$. The sensitivity is $S_{\varepsilon,max} = n_s\Lambda/100$. The coefficient is then

$$\eta = \frac{n_s\Lambda^2}{100\cdot\lambda}\left(\frac{\partial n_s}{\partial\lambda} - \frac{n_s}{\lambda}\right) \tag{33}$$

DOI:10.4186/ej.2024.28.8.33

where λ is the resonance wavelength and n_s is the refractive index at resonance. For the calculations in Fig. 8, the correction factor is approximately 1.0255. Here, the maximum sensitivity from Eq. (30) should be 6.435 nm per percent of strain. This is the limit shown in the figure when the volume fraction is reduced such that the effective index of the guiding region is low enough that the resonance is achieved at cut off condition. It is also clearly shown at lower film thickness in Fig. 8(b) for different low values of volume fraction. The graph shows that with volume fraction values as low as 0.01 the device operates near cut off even at larger film thickness values. Guided modes dominate (and hence lower the sensitivity) when increasing the volume fraction as expected. Figure 8(b) shows the cut off condition for different volume faction-film thickness configurations. As in the plot, the start of cut off and hence, maximum sensitivity, requires thicker film thickness at lower volume fraction of AgNPs, and vice versa. When the film thickness increase, particularly for larger volume fraction (> 0.04 in our case) the sensitivity to the strain starts to increase again. This could be due to the increase in the value of $\frac{\partial \beta_q}{\partial d}$ when moving towards more modes in the waveguide.

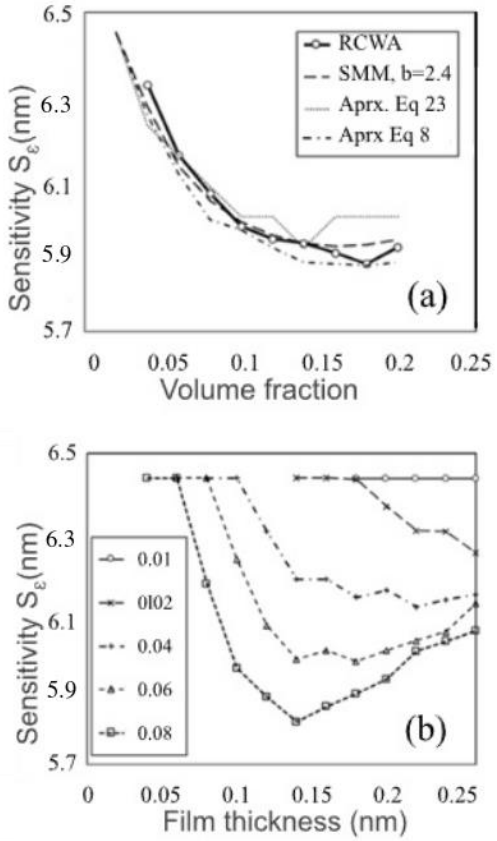

Fig. 8. (a) Strain sensitivity calculated using RCWA, SMM, and the approximated perturbation model in Eq. (12a) and 28. The SMM and the approximations are extended to lower volume fractions. (b) The approximate model shows the effect of the film thickness on the sensitivity for low volume fraction values.

Table 2. Sensitivity comparison between several recent publications and the proposed method in this paper.

Ref	**FOM** (1/RIU)	**Sensitivity** nm/RIU
This paper	-	Highest value reached is 6.435 nm per strain
[28]	839,666	252
[29]	1,571.4	550
[30]	FDTD 9,112 ($Q = 2.1 \times 10^4$) FMM ($Q = 3 \times 10^6$) 1.64×10^6	FDTD calculations 657 FMM calculations 656
[31]	-	Methane sensor 1427.3 Hemoglobin 1073.4 Toluene sensor 1019.7
[32]	FOM >50	Vary
[33]	35,889	1076.7

6. Conclusions

The work studied theoretically the use of polymer guided mode resonance devices for lateral strain sensing. The high index film is generated by adding AgNPs impurities in a thin layer of the polymer matrix. The effect of the high index film and nanoparticles concentration on the performance is studied. In the work, we present a fast model that estimates the GMR wavelength using the scattering matrix method. The model showed a performance that is 144 times faster than rigorous coupled wave analysis. The error between SMM and RCWA was minimized by modifying the effective index representation using averaging of refractive indices to a power of 2.4. This shows a very close agreement for the resonance due to the fundamental mode. However, the error for higher order modes increases. Using an approximate model utilizing Taylor expansion around resonance for a small value of strain, two approximate models were tested. The approximations show a maximum error of less than 3% when compared to both RCWA and SMM calculations. The maximum sensitivity using SMM and the approximate models show a maximum at cut-off that agrees with the predicted value that is linearly proportional to the grating period. The approximation, however, reduces the calculations cost with acceptable error compared to RCWA.

Below is the table comparison of sensitivity achieved in this paper and other recent publication. Noted that this paper is a theoretical investigation therefore FOM (figure of merit) is not calculated and the sensitivity obtained is in nm per strain.

Acknowledgement

The authors would like to extend our sincere thanks to Miss Pandhittaya Noikorn for providing the model calculation data using finite difference frequency domain (FDFD) method for this study.

References

[1] S. Foland, B. Swedlove, H. Nguyen and J. -B. Lee, "One-dimensional nanograting-based guided-mode resonance pressure sensor," *Journal of Microelectromechanical Systems*, vol. 21, no. 5, pp. 1117-1123, Oct. 2012.

[2] H. Guo *et al.*, "Vectorial strain gauge method using single flexible orthogonal polydimethylsiloxane gratings," *Scientific Reports*, vol. 6, no. 1, Mar. 2016.

[3] S. Wang, W. Guo, S. Qiu and M. D. McDonnell, "Performance of macro-scale molecular communications with sensor cleanse time," *2014 21st International Conference on Telecommunications (ICT)*, Lisbon, Portugal, 2014, pp. 363-368.

[4] K. F. Lei, K.-F. Lee, and M.-Y. Lee, "Development of a flexible PDMS capacitive pressure sensor for plantar pressure measurement," *Microelectronic Engineering*, vol. 99, pp. 1–5, Nov. 2012.

[5] S. Sarkar, S. Poulose, P. K. Sahoo, and J. Joseph, "Flexible and stretchable guided-mode resonant optical sensor: single-step fabrication on a surface engineered polydimethylsiloxane substrate," OSA Continuum, vol. 1, no. 4, pp. 1277 – 1286, Dec. 2018.

[6] L. M. Fortes, M. C. Gonçalves, and R. M. Almeida, "Flexible photonic crystals for strain sensing," *Optical Materials*, vol. 33, no. 3, pp. 408–412, Jan. 2011.

[7] H. Deb, N. Srisuai, S. Bonruang, R. Jolivot, C. Promptmas, and W. S. Mohammed, "3D-printed guided mode resonance readout system for biomedical and environmental applications," *Engineering Journal*, vol. 25, no. 6, pp. 35–43, Jun. 2021

[8] H. Fallah, L. Hakim, S. Boonruang, W. S. Mohammed, and S. H. Hsu, "Polymer-based guided-mode resonance sensors: From optical theories to sensing applications," *ACS Applied Polymer Materials*, vol. 5, no. 12, pp. 9700–9713, Nov. 2023

[9] Y. Bao, X. Liu, J. Hu, J. Zou, H. Han, and C. Wang, "Enhanced optical sensing performance in stacked resonant compound gratings," *Optics Express*, vol. 29, no. 18, p. 29458, Aug. 2021

[10] A. U. Rehman et al., "Three-dimensional modeling of the optical switch based on guided-mode resonances in photonic crystals," *Micromachines*, vol. 14, no. 6, p. 1116, May 2023

[11] M. Maleki and M. Mehran, "Guided-mode resonance sensors: different schemes for different applications," *Journal of the Optical Society of America. B, Optical Physics/Journal of the Optical Society of America. B, Online*, vol. 39, no. 6, p. 1634, May 2022

[12] A. C. Nkele and F. I. Ezema, *Diverse Synthesis and Characterization Techniques of Nanoparticles*. IntechOpen, 2021.

[13] Z. Liu and Y. Hu, "Sustainable antibiofouling properties of thin film composite forward osmosis membrane with rechargeable silver nanoparticles loading," *ACS Applied Materials & Interfaces*, vol. 8, no. 33, pp. 21666–21673, Aug. 2016.

[14] M. Hirsch, "Fiber optic microsphere with ZnO thin film for potential application in refractive index sensor—Theoretical study," *Photonics Letters of Poland*, vol. 10, no. 3, p. 85, Oct. 2018.

[15] J. Ji and Z. Li, "Tunable surface plasmon resonance wavelengths response from Au/Ag nanocomposite system," *Thin Solid Films*, vol. 764, p. 139602, Jan. 2023.

[16] X. Wang *et al.*, "Plasmonic effect of Ag/Au composite structures on the material transition," *Nanomaterials (Basel)*, vol. 12, no. 17, p. 2927, Aug. 2022.

[17] J. N. Reddy, *Introduction to the Finite Element Method*. Cambridge University Press eBooks, 2021.

[18] A. Taflove and S. C. Hagness, *Computational Electrodynamics: The Finite-Difference Time-Domain Method*. Boston: Artech House, 2005.

[19] R. C. Rumpf, *Electromagnetic and Photonic Simulation for the Beginner: Finite-Difference Frequency-Domain in MATLAB®*. Artech House, 2022.

[20] M. G. Moharam and T. K. Gaylord, "Rigorous coupled-wave analysis of planar-grating diffraction," *Journal of the Optical Society of America*, vol. 71, no. 7, p. 811, Jul. 1981.

[21] C. Altman and K. Suchy, *Reciprocity, Spatial Mapping and Time Reversal in Electromagnetics*. Dordrecht: Springer Netherlands, 1991.

[22] G. Morales-Luna, M. Herrera-Domínguez, E. Pisano, A. Balderas-Elizalde, R. I. Hernández-Aranda, and N. Ornelas-Soto, "Plasmonic biosensor based on an effective medium theory as a simple tool to predict and analyze refractive index changes," *Optics and Laser Technology*, vol. 131, p. 106332, Nov. 2020.

[23] R. C. Hibbeler, *Statics and Mechanics of Materials*. Pearson Prentice Hall, 2017

[24] A. Müller, M. C. Wapler, and U. Wallrabe, "A quick and accurate method to determine the Poisson's ratio and the coefficient of thermal expansion of PDMS," *Soft Matter*, vol. 15, no. 4, pp. 779–784, Jan. 2019.

[25] R. H. Alasfar, S. Ahzi, N. Barth, B. Кочкодан, M. Khraisheh, and B. Кочкодан, "A review on the modeling of the elastic modulus and yield stress of polymers and polymer nanocomposites: Effect of

temperature, loading rate and porosity," *Polymers (Basel)*, vol. 14, no. 3, p. 360, Jan. 2022.
[26] H. Deb, N. Srisuai, R. Jolivot, C. Promptmas, W. S. Mohammed, and S. Boonruang, "Enhanced sensitivity of guided mode resonance sensor through super-mode excitation at near cut-off diffraction," *Optics and Laser Technology*, vol. 132, p. 106517, Dec. 2020.
[27] P. B. Johnson and R. W. Christy, "Optical constants of the Noble Metals," *Physical Review*, vol. 6, no. 12, pp. 4370–4379, Dec. 1972.
[28] D. T. Cu, H.-W. Wu, H.-P. Chen, L.-C. Su, and C.-C. Kuo, "Exploiting thin-film properties and guided-mode resonance for designing ultrahigh-figure-of-merit refractive index sensors," *Sensors*, vol. 24, no. 3, p. 960, Feb. 2024
[29] C. Zhang, Y. Zhou, L. Mi, J. Ma, X. Wu, and Y. Fei, "High performance of a metal layer-assisted guided-mode resonance biosensor modulated by double-grating," *Biosensors*, vol. 11, no. 7, p. 221, Jul. 2021
[30] S. Mesli, H. Yala, M. Hamidi, A. BelKhir, and F. I. Baida, "High performance for refractive index sensors via symmetry-protected guided mode resonance," *Optics Express*, vol. 29, no. 14, p. 21199, Jun. 2021.
[31] M. Maleki and M. Mehran, "Guided-mode resonance sensors: different schemes for different applications," *Journal of the Optical Society of America. B, Optical Physics/Journal of the Optical Society of America. B, Online*, vol. 39, no. 6, p. 1634, May 2022.
[32] T. Smirnova *et al.*, "Resonant and sensing performance of volume waveguide structures based on polymer nanomaterials," *Nanomaterials*, vol. 10, no. 11, p. 2114, Oct. 2020.
[33] L. Qian, T. Gu, S. Xu, X. Zhang, and K. Wang, "Guided-mode resonance sensors with ultrahigh bulk sensitivity and figure of merit assisted by a metallic layer and structural symmetry-breaking," *Optics Express*, vol. 31, no. 2, p. 1844, Jan. 2023.

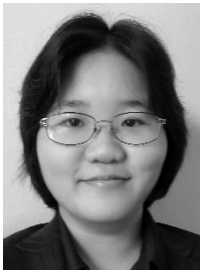

Pundharika Noikorn graduated from the department of mechanical and aerospace engineering, King Mongkut University of Technology North Bangkok, Thailand in 2019. She is currently a graduate student in Electrical and Computer Engineering at Bangkok University, Pathumthani, Thailand.

Sakoolkan Boonruang graduated from the department of electrical engineering, King Mongkut Institute of Technology Ladkrabang, Thailand in 1999. In 2002, she joined the college of optics and photonics, CREOL, University of Central Florida, USA, as a graduate student. She received her Ph.D. degree in optics in 2007 with thesis titled "Two-dimensional Guided Mode Resonant Structures for Spectral Filtering Applications" under the supervision of Prof. M. G. Moharam. In the same year, she returned to Thailand and joined the National Electronics and Computer Technology research center (NECTEC), where she is currently a researcher. Her current work focuses on fabrication of one/two dimensional periodical structures, optical sensors, VOCs sensor and biomedical optics applications.

Waleed S. Mohammed graduated from the department of electronics and electrical communications, Faculty of engineering, Cairo University, Giza, Egypt on 1996 with a major in control systems. In 1997, he joined the Lasers institute (NILES), Cairo University as a teaching assistant. He received M.Sc. degree from the department of computer engineering, Cairo University in 1999. In the same year he joined the College of optics and photonics/CREOL, University of Central Florida, Orlando, FL, USA as a research assistant. In 2001, he received M.Sc. degree in optics in 2001. He completed his Ph.D. work in 2004 and his thesis was titled "nano/micro-optical elements for mode coupling applications. In 2004, he joined Prof. P. W. E. Smith's ultra-fast photonics laboratory (UPL), Electrical and Computer Engineering department, University of Toronto, as a postdoctoral fellow. In 2005, he joined Prof. Li Qian's group at the same university. In 2007 Dr. Mohammed joined the International School of Engineering, Chulalongkorn University, Bangkok, Thailand as an instructor in the nano-engineering department. He taught optoelectronics, fundamental of optics, numerical modeling, nano-electronics and research methodology. As of September 2010, He joined the school of Engineering, Bangkok University as a research scholar).